Seismic image reconstruction using complex wavelets

Mark A. Miller[a], Nick G. Kingsbury[a] and Richard W. Hobbs[b]

[a] University of Cambridge, Department of Engineering, Trumpington Street, Cambridge CB2 1PZ, United Kingdom;

[b] Department of Earth Sciences, University of Durham, Science Laboratories, South Road, Durham DH1 3LE, United Kingdom

ABSTRACT

The aim of seismic imaging is to reconstruct subsurface reflectivity from scattered acoustic data. In standard reconstruction techniques, the reflectivity model parameters are usually defined as a grid of point scatterers over the area or volume of the subsurface to be imaged. We propose an approach to subsurface imaging using the Dual Tree Complex Wavelet Transform (DT-CWT) as a basis for the reflectivity. This basis is used in conjunction with an iterative optimization which frames the problem as a linearized inverse scattering problem. We demonstrate the method on synthetic data and a marine seismic data set acquired over the Gippsland Basin near Australia. The technique is shown to reduce noise and processing artifacts while preserving discontinuities. It is likely to be particularly useful in cases where the acquired date is incomplete.

Keywords: Seismic, image reconstruction, wavelet, migration

1. INTRODUCTION

The objective of marine seismic imaging is to reconstruct subsurface reflectivity from acoustic observations normally taken near the sea surface. This can be achieved by iteratively minimizing a cost function consisting of a data matching term and a regularization term. In seismic processing literature the procedure is usually termed least-squares migration (LSM).

LSM has been shown to be effective in optimizing the reconstruction of subsurface reflectivity, particularly in cases of incomplete data.[1,2] There are several cases where a data set may be incomplete: finite recording apertures, coarse source/receiver distribution, gaps between recording lines for 3D imaging and poor subsurface illumination caused by irregular ray coverage due to strong lateral variations in velocity.

In seismic image reconstruction applications, subsurface reflectivity is usually defined on a grid of point reflectors. We propose using a complex wavelet basis called the Dual Tree Complex Wavelet Transform (DT-CWT)[3] for the reflectivity. This introduces limited redundancy (2m:1 for m-dimensional signals) and allows the transform to provide approximate shift invariance and directionally selective filters (properties lacking in the traditional wavelet transform) while preserving the usual properties of perfect reconstruction and computational efficiency.

Wavelet bases tend to decorrelate or diagonalize a range of non-stationary signals. This has led to extensive use of wavelet bases in the area of information coding and compression. In LSM, diagonalization of the model space allows a more accurate and practical representation of prior information about the model parameters. This prior information is incorporated in the regularization term of the cost function that is minimized.

Using more sophisticated regularization becomes more important for missing or undersampled data problems or when increased resolution is required in the reflectivity model to be reconstructed. Alternatively, relaxing sampling requirements can reduce the cost of data acquisition.

The main drawback of LSM is its computational cost. It is an iterative method with a high computational overhead relative to some other migration schemes. In light of this, LSM is best suited to target oriented applications, where a smaller area or volume of interest is reconstructed after an initial reconnaissance using another non-iterative migration technique.[4]

M.A.M.: E-mail: mam59@cam.ac.uk, N.G.K.: E-mail: ngk@eng.cam.ac.uk, R.W.H.: E-mail:r.w.hobbs@durham.ac.uk

Computational Imaging III, edited by Charles A. Bouman, Eric L. Miller,
Proceedings of SPIE-IS&T Electronic Imaging, SPIE Vol. 5674

Wavelet bases have been successfully applied to other linearized inverse problems[5] including linear inversion with application to well logging.[6,7] Herrmann employed curvelet/contourlet transforms for seismic imaging similar to that described here but took a minimax-style approach.[8] The use of a complex wavelet transform with similar properties to the DT-CWT in seismic processing was suggested by Fernandes.[9] De Rivaz and Kingsbury used the DT-CWT in a similar manner to here for image restoration.[10]

2. DUAL TREE CWT

Choosing a basis that is appropriate for the statistical characteristics of a particular class of input signal is a classical problem. Linear transforms have proven to be popular due to their simplicity and mathematical tractability. The DT-CWT is a derivative of the discrete wavelet transform that generates complex coefficients by using a dual tree of wavelet filters to obtain their real and imaginary parts. Here the Q-shift version of the DT-CWT is chosen as the wavelet basis for its key advantages compared to other wavelet transforms. These are summarized as follows:[3]

1. **Shift invariance:** Eliminates aliasing defects.
2. **Good directional selectivity:** The DT-CWT has six directionally selective subbands in 2 dimensions and 28 in 3 dimensions.
3. **Basis vectors form an almost tight frame:** Allows use of the transform in the efficient Conjugate Gradient Descent (CGD) algorithm.
4. **Perfect reconstruction:** No distortion caused by the forward transform followed by the inverse transform.
5. **Limited redundancy:** Redundancy is independent of the number of scales and limited to 2^n for n dimensions.
6. **Efficient computation:** Filters are separable and computation is less than 2^n times that of the simple DWT for n dimensions.

The first point is well known to provide superior denoising performance and often leads designers to use undecimated transforms.[11,12] However, as shown by Kingsbury the DT-CWT can outperform undecimated real wavelet transforms because the DT-CWT's improved directional selectivity (point 2) provides better denoising near nonvertical and nonhorizontal edges or lines.[11] Points 3 and 4 are important in order to avoid any noise or error amplification effects when repeatedly performing forward and inverse transforms such as in the conjugate gradient algorithm used here. Points 5 and 6 lead to lower algorithm complexity and increased speed.

3. SEISMIC MODELLING

Using the high-frequency single-scattering Born approximation the seismic data can be modeled using a generalized Radon transform:

$$\mathbf{d} = \mathbf{L}\mathbf{m} + \mathbf{n} \tag{1}$$

In (1) $\mathbf{d}$ is the observed scattered acoustic data which is a function of time and acoustic source and receiver positions. $\mathbf{m}$ is the reflectivity on a regular grid in 2 or 3 dimensions and $\mathbf{L}$ is the linearized seismic modeling operator mapping from one to the other.[1] Observed data not modeled by the linear operator is modeled by additive noise $\mathbf{n}$ assumed to be Gaussian distributed with covariance $\mathbf{C_n}$. Thus, equation (1) is an inverse problem where the objective is to recover the reflectivity $\mathbf{m}$ from the observed data $\mathbf{d}$.

The data is modeled using a ray based method where the sound velocity profile is approximated by a smooth background velocity profile plus a perturbation. Our approach is equivalent to a linearized inversion of the reflectivity for a given background velocity distribution. We write $\mathbf{d} = \mathbf{L}\mathbf{m}$ as:

$$\mathbf{d}(t,p) = \sum_{\mathbf{r}} \mathbf{m}(\mathbf{r}) A(\mathbf{r},\mathbf{s},\mathbf{g})(w \circledast \zeta)(t - \tau(\mathbf{r},\mathbf{s},\mathbf{g})) \tag{2}$$

p and t denote the particular source/receiver combination or trace and the discrete time along the trace respectively. w is the source wavelet recorded at the surface including the additional sea surface reflection or 'ghost'. ζ is the wavelet shaping factor which is a differentiator in 3D and a half-differentiator in 2D. $\circledast$ denotes convolution in time. τ is the 2-way travel time from the source location $\mathbf{s}$ to the reconstruction point $\mathbf{r}$ and back to the geophone (receiver) $\mathbf{g}$. The travel times are generated using the eikonal equations and the assumed background velocity field. This can be done using the open source seismic modeling program, Seismic Unix.[13] A is the amplitude of the ray incorporating geometrical spreading and an angle dependant obliquity factor.[14]

$\mathbf{L^T}$ is the equivalent matrix transpose of (2), so we write $\mathbf{m}_{Kirch} = \mathbf{L^T d}$ as:

$$\mathbf{m}_{Kirch}(\mathbf{r}) = \sum_p \sum_t \mathbf{d}(t,p) A(\mathbf{r},\mathbf{s},\mathbf{g}) (w \circledast \zeta)(t - \tau(\mathbf{r},\mathbf{s},\mathbf{g})) \tag{3}$$

Equation (3) forms the basis of the current standard industry approach to seismic imaging known as Kirchhoff migration. In this approach $\mathbf{L^T}$ is used to approximate $\mathbf{L}^{-1}$.

3.1. Computational Aspects of L and $\mathbf{L^T}$

Assuming that the size of the (2D) model $\mathbf{m}$ is $N_x \times N_z$ and there are N_p recorded waveforms (traces) and N_t time samples per trace so that $\mathbf{d}$ is of length $N_p N_t$, then brute force matrix multiplication by $\mathbf{L}$ or $\mathbf{L^T}$ would require approximately $N_x N_z N_p N_t$ operations. This is likely to be unacceptably large. Fortunately $\mathbf{L}$ may be regarded as the cascade of a sparse matrix multiplication and a relatively efficient convolution process, summarized as follows.

In equation (2) we see that each point in the model $\mathbf{m}$ excites each recorded waveform with a band-limited impulse of short duration, at a point determined by the total propagation delay from source to receiver via that point in $\mathbf{m}$, τ. In applying $\mathbf{L}$ these short pulses may be added to the traces in turn, and only affect a proportion α of the total traces in which the path delay lies within the range of delays being measured in $\mathbf{d}$. Interpolated pulse waveforms are used to synthesize fractional sample delays and the pulses are N_s samples long. Each pulse is scaled by an appropriate attenuation coefficient, dependent on the path. This all requires approximately $\alpha N_x N_z N_s N_p$ operations.

Each trace is then convolved with the combined source wavelet and wavelet shaping factor. This is typically performed in the frequency domain and requires of order $N_p N_t \log_2(N_t)$ operations, significantly less processing than the previous step.

Thus, $\mathbf{L}$ is the cascade of a sparse matrix multiplication and a relatively efficient convolution process. Hence the total processing is of order $N_s N_x N_z N_p$ operations. Note that this is much greater than the DT-CWT of the model, which is approximately $100 N_x N_z$ operations in 2D. Applying the adjoint operator $\mathbf{L^T}$ to $\mathbf{d}$ requires the same amount of computation as applying the forward operator.

4. BAYESIAN INVERSION USING A WAVELET BASIS

Expressing the reflectivity using wavelet basis functions by substituting $\mathbf{m} = \mathbf{Pw}$ in (1) results in equation (4).

$$\mathbf{d} = \mathbf{LPw} + \mathbf{n} \tag{4}$$

In (4) $\mathbf{w}$ are the lexographically ordered wavelet coefficients whose real and imaginary parts are treated as separate variables. Starting with equation (4), we derive in a Bayesian framework a cost function which when minimized provides a *maximum a posteriori (MAP)* estimate for the wavelet coefficients $\mathbf{w}$. The conditional probability for the data given the wavelet coefficients is:

$$p_{\mathbf{d}|\mathbf{w}}(\mathbf{d}|\mathbf{w}) = \frac{1}{(2\pi\,|\mathbf{C_n}|)^{1/2}} \exp\left\{ -\frac{1}{2} (\mathbf{LPw} - \mathbf{d})^T \mathbf{C_n}^{-1} (\mathbf{LPw} - \mathbf{d}) \right\} \tag{5}$$

The MAP estimate for the coefficients is presented in equation (6) and manipulated into a more convenient form using Bayes theorem.

$$\begin{aligned}
\mathbf{w}_{MAP} &= \arg\max_{\mathbf{w}} \left\{ p_{\mathbf{w}|\mathbf{d}}(\mathbf{w}|\mathbf{d}) \right\} \\
&= \arg\max_{\mathbf{w}} \left\{ p_{\mathbf{d}|\mathbf{w}}(\mathbf{d}|\mathbf{w})\, p_{\mathbf{w}}(\mathbf{w}) \right\} \\
&= \arg\min_{\mathbf{w}} \left\{ -\log\left(p_{\mathbf{d}|\mathbf{w}}(\mathbf{d}|\mathbf{w})\, p_{\mathbf{w}}(\mathbf{w}) \right) \right\} \\
&= \arg\min_{\mathbf{w}} \left\{ (\mathbf{LPw} - \mathbf{d})^T\, \mathbf{C_n}^{-1}\, (\mathbf{LPw} - \mathbf{d}) + f(\mathbf{w}) \right\}
\end{aligned} \tag{6}$$

where $f(\mathbf{w}) = -\log\left(p_{\mathbf{w}}(\mathbf{w})\right)$ is the regularization term. Our prior model for the wavelet coefficients assumes the real and imaginary parts have independent Gaussian distributions with zero mean and known variance. Thus $f(\mathbf{w})$ becomes:

$$f(\mathbf{w}) = \mathbf{w}^T \mathbf{C_w}^{-1} \mathbf{w} \tag{7}$$

and we obtain an estimate for the wavelet coefficients by minimizing:

$$\mathbf{E_w}(\mathbf{w}) = (\mathbf{LPw} - \mathbf{d})^T\, \mathbf{C_n}^{-1}\, (\mathbf{LPw} - \mathbf{d}) + \mathbf{w}^T \mathbf{C_w}^{-1} \mathbf{w} \tag{8}$$

We compare this to the case where a wavelet basis is not used. The relevant cost function is:

$$\mathbf{E_m}(\mathbf{m}) = (\mathbf{Lm} - \mathbf{d})^T\, \mathbf{C_n}^{-1}\, (\mathbf{Lm} - \mathbf{d}) + f(\mathbf{m}) \tag{9}$$

but a representative $f(\mathbf{m})$ is now more difficult to define.

As stated in section 3 traditional migration in its most basic form is equivalent to estimating the reflectivity by applying the transpose of the forward modeling operator to the observed data. Note that this is equivalent to one iteration of a steepest descent or conjugate gradient minimization procedure like that described here.

5. ALGORITHM

We now turn to the implementation of the algorithm. To speed up convergence and allow estimation of the coefficient variances, we start with a non-iterative estimate for the reflectivity. If the available estimate $\tilde{\mathbf{m}}_\mathbf{0}$ is not scaled correctly, it is multiplied by λ that minimizes $\mathbf{E_m}(\lambda\tilde{\mathbf{m}}_\mathbf{0})$ with $f(\mathbf{m}) = 0$, so that $\mathbf{m_0} = \lambda\tilde{\mathbf{m}}_\mathbf{0}$. This is equivalent to performing one iteration of steepest descent minimization of (9) with $\tilde{\mathbf{m}}_\mathbf{0}$ as the search direction and no regularization or preconditioning.

Following De Rivaz and Kingsbury[10] the coefficient variances are allowed to vary within each subband but are the same for the real and imaginary parts of a given coefficient. These variances are estimated from the forward DT-CWT of the initial reflectivity estimate $\mathbf{w_0} = \mathbf{P^T m_0}$ as $\sigma_i^2 = 0.5|w_i|^2$ where w_i is the corresponding complex wavelet coefficient in $\mathbf{w_0}$.

The algorithm is initialized with $\mathbf{w_0}$ and the energy function (8) is minimized using a preconditioned CGD algorithm optimized to use the minimum number of forward and transpose seismic modeling operators per iteration (one of each), since these operations comprise the bulk of the computational effort. A block diagram illustrating the algorithm implementation is displayed in figure 1. Figure 1(a) shows the preprocessing as detailed in this section, while figure 1(b) contains the optimized conjugate gradient loop, where the steepest descent direction is updated at each iteration rather than recalculated from scratch.

After sufficient iterations the reflectivity estimate is found by applying the inverse wavelet transform to the current coefficient estimate:

$$\hat{\mathbf{m}} = \mathbf{P}\hat{\mathbf{w}}_k \tag{10}$$

Note that the matrices $\mathbf{P}$ and $\mathbf{P^T}$ required in the conjugate gradient algorithm are not implemented as matrix multiplications but using much faster wavelet decomposition and reconstruction algorithms.

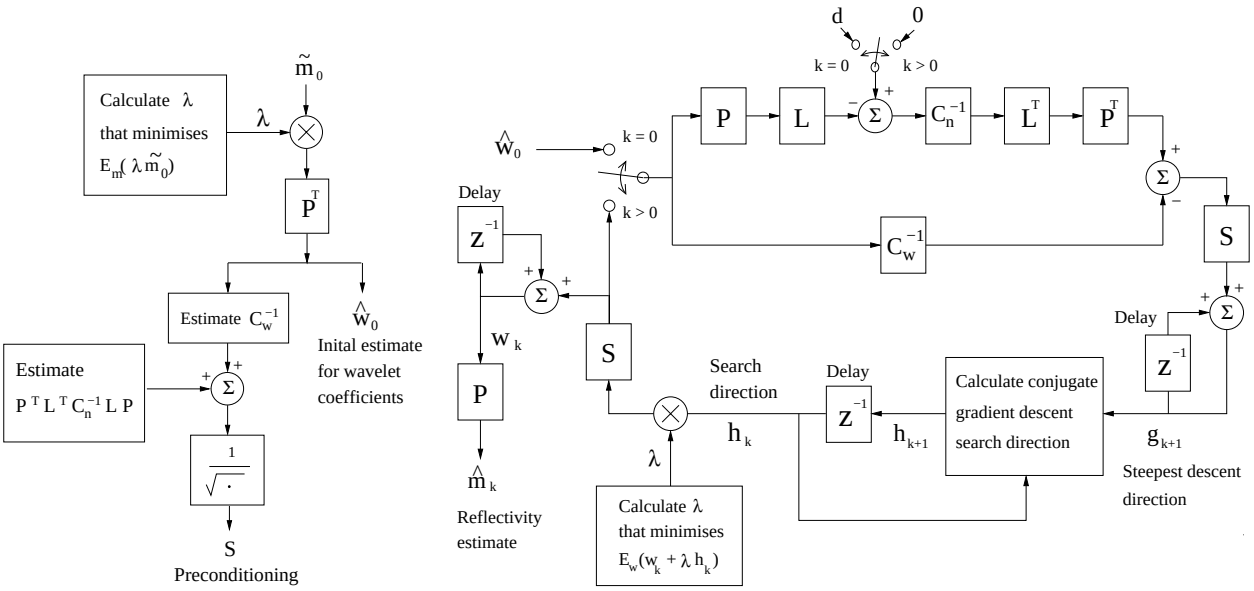

(b) Preprocessing (c) Iterative algorithm

Figure 1. Block diagram of the complex wavelet seismic imaging system

An area where the use of a wavelet basis makes the inversion more difficult is the preconditioning of the system. To speed up convergence, CGD algorithms used to solve linear inversion problems are preconditioned by scaling the variables prior to minimization. In its usual form the diagonal elements of the Hessian of the cost function $\bigtriangledown^2\mathbf{E}$ need to be calculated, so that they can be scaled to unity by the preconditioning. For the non-wavelet cost function (9), ignoring the regularization term ($f(\mathbf{m}) = 0$), the Hessian is:

$$\bigtriangledown^2\mathbf{E_w} = \mathbf{L^T C_n}^{-1}\mathbf{L} \tag{11}$$

However, for wavelet based inversion this becomes:

$$\bigtriangledown^2\mathbf{E_m} = \mathbf{P^T L^T C_n}^{-1}\mathbf{LP} \tag{12}$$

Calculating the diagonal elements of (12) is more difficult. Fortunately, for preconditioning the exact values are not required and a rough estimate is sufficient. The computational effort required to obtain these values can be significantly reduced by using heavy interpolation of the wavelet subbands, taking advantage of the small support of most of the wavelet basis functions, and by decimation of the trace locations for large data sets.

6. RESULTS AND CONCLUSIONS

6.1. Synthetic Data

The synthetic data shown in figure 3 was generated using Seismic Unix.[13] This sparse dataset consists of six common shot gathers spaced at 300m with 30 traces (lines of data for particular source/geophone combinations) in each gather. The maximum offset from source to receiver in each gather is 1500m. The background velocity field is linearly increasing with depth from $1500ms^{-1}$ at depth 0 at a rate of $0.8ms^{-1}$ per meter. The reflectors used to generate the data are displayed in figure 3(a).

Seismic Unix Kirchhoff depth migration is used to obtain an initial estimate of the reflectivity. The Kirchhoff migrated section is shown in figure 3(b). LSM with complex wavelets is now applied to the problem and the result after 10 iterations is displayed in figure 3(c).

We also compare the result to that obtained with non-wavelet least-squares migration using the cost function in equation (9) with the regularization defined as $f(\mathbf{m}) = \mathbf{m}^T C_{\mathbf{m}}^{-1}\mathbf{m}$, where $C_{\mathbf{m}} = \sigma_{\mathbf{m}}^2\mathbf{I}$ as suggested by Duijndam *et al.*.[15] $\sigma_{\mathbf{m}}^2$ is the variance of the reflectivity model parameters, which we have estimated as the sample variance of the initial Kirchhoff estimate. As for the wavelet based conjugate gradient algorithm, preconditioning is used and the estimate is initialized using the Kirchhoff migration result.

The complex wavelet LSM method in figure 3(c) shows improvement in terms of noise and artifact reduction over both the Kirchhoff migration and the non-wavelet LSM method. This is to be expected, as the wavelet method uses a greater amount of prior information, but it does demonstrate the potential of the method.

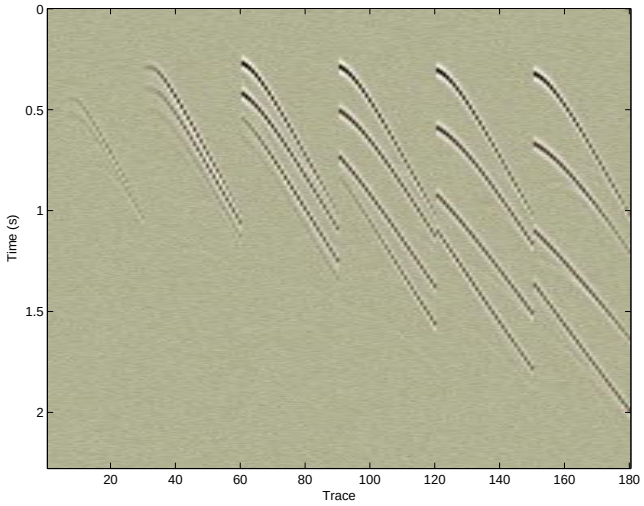

Figure 2. Synthetic data generated using Seismic Unix

6.2. Gippsland Basin Data

The data used in the following results are from a 3-D survey acquired in 2001 over the offshore Gippsland Basin near Australia. A single shot/streamer line was selected from the data volume to test the complex wavelet least-squares migration algorithm in 2 dimensions. From this 14216 traces with source/receiver midpoints along a length of 2km above the area to be imaged are used.

The noise covariance matrix is assumed to be diagonal and the noise variances are estimated directly from the trace data. The estimates consist of two components. The first, which models background noise due to incoherent scatterers, was picked roughly by hand, with variance estimates decaying with time and slowly with source/receiver offset. The second is proportional to a windowed average of the data values squared along each trace. This component models the modeling error which is assumed to be roughly proportional to the data at similar travel times.

For our results we used the Kirchhoff based estimate $\tilde{\mathbf{m}}_\mathbf{0} = \mathbf{R}^{-1}\mathbf{L}^\mathbf{T}{\mathbf{C}_\mathbf{n}}^{-\mathbf{1}}\mathbf{d}$ to initialize the algorithm, where $\mathbf{R}$ is diagonal with diagonal entries R_{ii} equal to those of the Hessian of the non-wavelet LSM cost function with no constraint term, *i.e.* $R_{ii} = [\mathbf{L}^\mathbf{T}{\mathbf{C}_\mathbf{n}}^{-\mathbf{1}}\mathbf{L}]_{ii}$. We demonstrate the algorithm's ability to cope with undersampled data by using a reduced data set where the traces are decimated by a factor of 10. In the absence of any ground truth data, we compare the result to the Kirchhoff based estimate obtained using the full data set. As for the synthetic data, we compare the result to that obtained with non-wavelet least-squares migration using the cost function in (9) with the regularization defined as $f(\mathbf{m}) = \mathbf{m}^T C_{\mathbf{m}}^{-1}\mathbf{m}$, where $C_{\mathbf{m}} = \sigma_{\mathbf{m}}^2\mathbf{I}$.

Figure 4 displays the results for an approximately 1.7km wide by 0.8km deep target area. Figure 4(a) contains the Kirchhoff estimate for the decimated data used to initialize the complex wavelet system. Noise and so called migration artifacts are visible due to the sparsity of the data. Our pseudo ground-truth data, the Kirchhoff reconstruction using the full data set in figure 4(c), suppresses much although not all of the noise seen in the

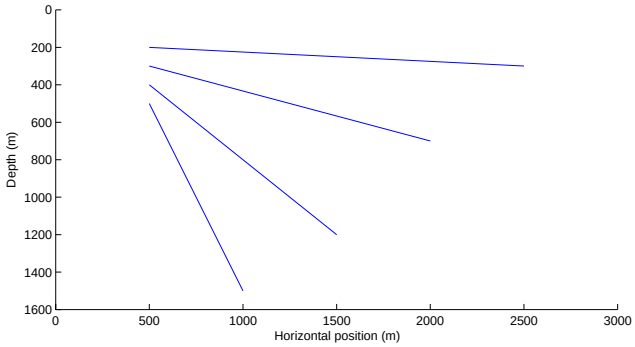

(a) Dipping reflectors used to generate synthetic data

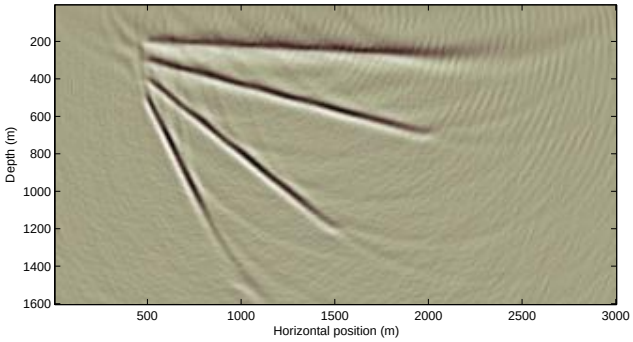

(b) Seismic Unix Kirchhoff migration

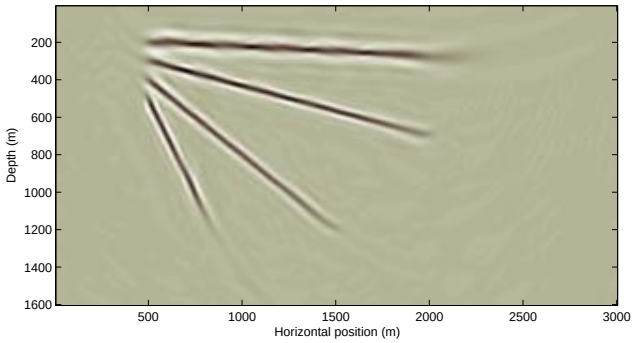

(c) 10 iterations of complex wavelet LSM

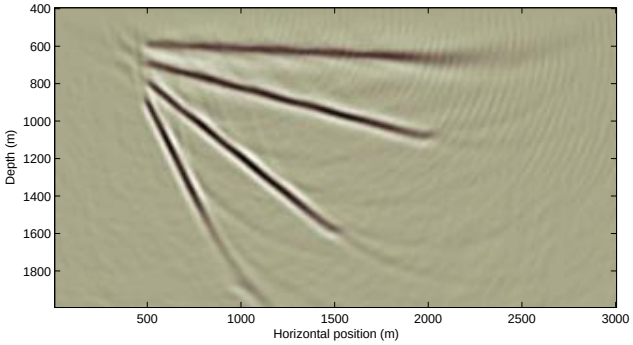

(d) 10 iterations of non-wavelet LSM

Figure 3. Results for the synthetic data generated in Seismic Unix

reconstruction using the decimated data. The result for the complex wavelet system on the decimated data in figure 4(b) is seen to significantly suppress noise and reduce migration artifacts seen in figure 4(a) while enhancing reflectors.

The non-wavelet iterative algorithm (figure 4(d)) also enhances the subsurface reflectors but is not as well regularized and does not suppress noise and artifacts as well as the complex wavelet system. The non-wavelet algorithm diverges in just a few iterations if no regularization is employed. The results for the complex wavelet system presented here are stable *i.e.* continuing for more iterations brings increasingly smaller updates to the estimate and the reflectivity estimate does not diverge.

7. ACKNOWLEDGEMENTS

The Authors acknowledge the support of ExxonMobil, who provided the data from the Gippsland Basin marine seismic survey. We are also grateful for financial support from the New Zealand Vice Chancellors Committee, Canterbury University, New Zealand and Trinity College, Cambridge, UK.

REFERENCES

1. T. Nemeth, C. Wu, and G. T. Schuster, "Least-squares migration of incomplete reflection data," *Geophysics* **64**(1), pp. 208–221, 1999.
2. B. Duquet, K. J. Marfurt, and J. A. Dellinger, "Kirchhoff modeling, inversion for reflectivity, and subsurface illumination," *Geophysics* **65**(4), pp. 1195–1209, 2000.

3. N. G. Kingsbury, "Complex wavelets for shift invariant analysis and filtering of signals," *Journal of Applied and Computational Harmonic Analysis* **10**, pp. 234–253, May 2001.
4. Z. Jiang and G. T. Schuster, "Target oriented least-squares migration," in *73rd Ann. Internat. Meeting, Soc of Expl. Geophys., Expanded Abstracts*, pp. 1043–1046, (Dallas, TX), Oct 2003.
5. E. L. Miller and A. S. Willsky, "A multiscale, statistically-based inversion scheme for the linearized, inverse scattering problem," *IEEE Transactions on Geoscience and Remote Sensing* **34**(2), pp. 346–357, 1996.
6. X. Li, M. D. Sacchi, and T. J. Ulrych, "Wavelet transform inversion with prior scale information," *Geophysics* **61**(5), pp. 1379–1385, 1996.
7. J. A. Kane and a F. J. Herrmann, "Wavelet domain linear inversion with application to well logging," in *71st Ann. Internat. Meeting, Soc of Expl. Geophys., Expanded Abstracts*, pp. 694–697, (San Antonio, TX), Sep 2001.
8. F. J. Herrmann, "Multifractional splines: application to seismic imaging," in *Proceedings of SPIE*, **5207**, pp. 240–258, (San Diego, CA), Nov 2003.
9. F. C. A. Fernandes, *Shift-Insensitive, Complex Wavelet Transforms with Controllable Redundancy*. PhD thesis, Electrical and Computer Engineering, Rice University, Aug 2001.
10. P. de Rivaz and N. Kingsbury, "Bayesian image deconvolution and denoising using complex wavelets," in *IEEE International Conference on Image Processing*, **2**, pp. 273–276, Oct 2001.
11. N. G. Kingsbury, "The dual-tree complex wavelet transform: a new efficient tool for image restoration and enhancement," in *Proc. European Signal Processing Conference*, pp. 319–322, (Rhodes, Greece), Sep 1998.
12. R. R. Coifman and D. L. Donoho, "Translation invariant denoising," in *Wavelets and Statistics, Lecture notes in Statistics*, A. Antoniadis and G. Oppenheim, eds., **103**, pp. 125–150, Springer Verlag, New York, 1995.
13. J. K. Cohen and J. Stockwell, *SWP/SU: Seismic Unix Release 37: a free package for seismic research and processing*, Centre for Wave Phenomena, Colorado School of Mines, 2003.
14. O. Yilmaz, *Seismic Data Analysis*, Society of Exploration Geophysicists, Tulsa, OK, 2001.
15. A. J. W. Duijndam, A. W. F. Volker, and P. M. Zwartjes, "Reconstruction as an efficient alternative for least squares migration," in *70th Ann. Internat. Meeting, Soc of Expl. Geophys., Expanded Abstracts*, pp. 1012–1015, (Calgary, Cananda), Aug 2000.

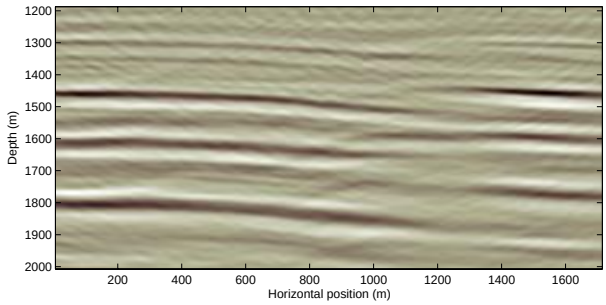

(a) Initial Kirchhoff estimate - decimated data

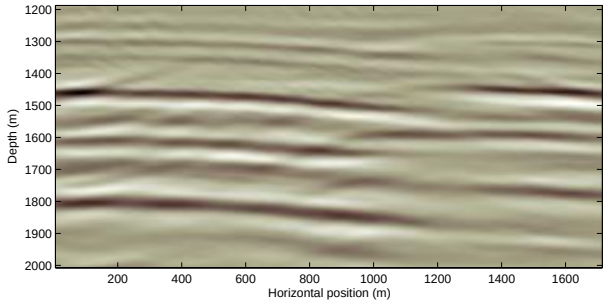

(b) 10 iterations of complex wavelet imaging - decimated data

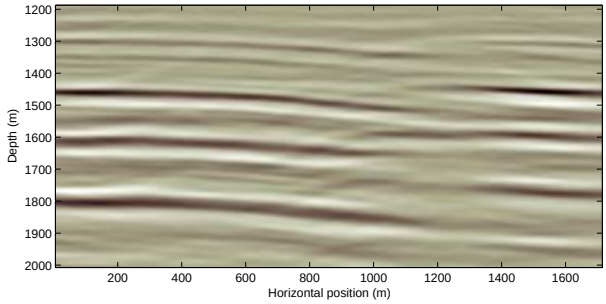

(c) Kirchhoff estimate - full data set

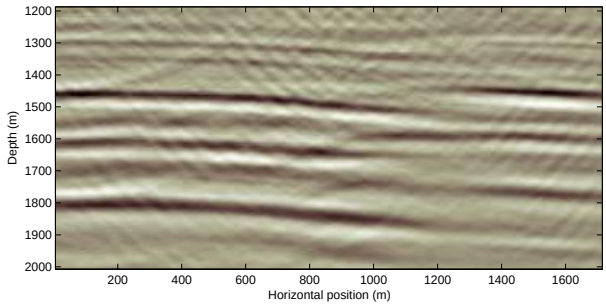

(d) Non-wavelet LSM - decimated data

Figure 4. Results for the Gippsland data set